

1 **Computation of Flexoelectric Coefficients of a MoS₂ monolayer with a**
2 **Model of Self-consistently Distributed Effective Charges and Dipoles**

3 Yida Yang, Laurent Hirsinger, and Michel Devel^{a)}
4 *FEMTO-ST institute, UBFC, CNRS, ENSMM, 15B*
5 *avenue des Montboucons, 25030 Besançon CEDEX,*
6 *France*

Flexoelectricity is an electromechanical coupling phenomenon, that can generate noticeable electric polarization in dielectric materials for nanoscale strain gradients. It is gaining an increasing attention because of its potential applications, and the fact that experimental results were initially an order of magnitude higher than initial theoretical predictions. This stimulated intense experimental and theoretical researches to investigate flexoelectric coefficients in dielectric materials such as two-dimensional materials. In this work, we concentrate on the calculation of the flexoelectric coefficients of 2D-MoS₂ thanks to a model using self-consistently determined charges and dipoles on the atoms. More specifically, we study the importance of two contributions which were neglected/omitted in previous papers using this model, namely the charge term in the total polarization and the conservation of electric charge through a Lagrange multiplier. Our calculations demonstrate that the results for flexoelectric coefficients computed with this improved definition of polarization agree better with experimental measurements, provided consistent definitions for signs are used. Additionally, we show how two physical contributions with opposite signs compete to give net values of flexoelectric coefficients that can be either positive **or** negative depending on their relative importance, and give net values for the case of MoS₂.

^{a)}Electronic mail: michel.devel@femto-st.fr

7 I. INTRODUCTION

8 Flexoelectricity¹, a fascinating electromechanical phenomenon, is widely em-
9 ployed to describe electric polarization caused by strain gradient. Unlike piezo-
10 electricity, which arises only in noncentrosymmetric materials, flexoelectricity can
11 a priori exist in all materials. Therefore, flexoelectricity can provide new oppor-
12 tunities to use some centrosymmetric materials to build electromechanical sys-
13 tems, such as energy harvesters^{2,3}, actuators^{4,5}, flexible electronics⁶, flexoelectric
14 sensors^{7,8}.

15 Flexoelectricity was first predicted by Mashkevich and Tolpygo⁹ during Tolpygo's
16 studies on the optical and elastic properties of crystals. The polarization due to
17 the flexoelectric effect was later phenomenologically described by Kogan¹⁰, using
18 the contraction of a fourth order flexoelectricity tensor with the third order strain
19 gradient tensor. Ever since the terminology 'flexoelectricity' was firstly borrowed
20 from the liquid crystals community by Indenbom^{11,12} et al in 1981, a great deal
21 of theoretical work has been done to advance the development of the theory of
22 flexoelectricity in solids. Earlier theoretical descriptions principally concentrated
23 on lattice dynamics using Kogan's phenomenological theory^{10,13,14} and continuum
24 mechanics¹⁵ or microscopic theories based on lattice dynamics^{13,16-18} and quantum
25 mechanics¹⁹⁻²². Calculations used methods such as core-shell model^{17,23}, rigid-ion
26 model^{13,14}, molecular dynamics simulations²⁴⁻²⁶, finite element method^{27,28} and
27 phase-field method²⁹. Recently, the advancement and popularity of machine
28 learning techniques³⁰⁻³² provide original means for the computation of flexoelec-
29 tricity coefficients. **Another strategy combining isogeometric analysis (IGA) and**
30 **the Method of Moving Asymptotes (MMA) allows to extract both the real and**
31 **complex parts of the piezoelectric and flexoelectric coefficients from electrical**
32 **impedance curves³⁴. This complements another technique based on topology op-**
33 **timization methods to design multi-material flexoelectric structures, using the**
34 **electromechanical coupling coefficient as figure of merit³³.**

35 Flexoelectricity in solids was believed to be a very small effect. However, at
36 the beginning of the 2000s, Ma and Cross reported unexpectedly high experimen-
37 tal flexoelectric responses in a variety of perovskite ceramics^{35–40} greatly arousing
38 the interest in research of flexoelectricity in perovskite ceramics.^{41–43} Furthermore,
39 the relative importance of the flexoelectric effect with respect to the piezoelectric
40 effect should increase as the scale of strain inhomogeneities decreases. Therefore,
41 the recent development of ultrathin (2D) nanomaterials, due to the desired need
42 for miniaturized devices, provide opportunities for researchers to study flexoelec-
43 tricity in 2D materials which could offer interesting electromechanical coupling
44 in nanodevices. Such an interest has stimulated intense research to investigate
45 flexoelectric coefficients in carbon nanomaterials^{20,21,44–46} (nanotubes, fullerenes,
46 nanocores and patterned graphene), phosphorene⁴⁷, hexagonal boron nitride⁴⁸ and
47 transition-metal dichalcogenides^{49,50} by means of first-principle calculations. Re-
48 markably, Kumar et al very recently calculated the flexoelectric coefficient for
49 fifty-four representative atomic monolayers selected from distinct groups in the
50 periodic table of elements using ab-initio Density Functional Theory (DFT)⁵¹.

51 Recently, Zhuang and co-workers used molecular dynamics simulations cou-
52 pled with a charge dipole (QP) model to compute flexoelectric coefficients for
53 transition-metal dichalcogenides⁵² and related materials⁵³. This kind of method
54 uses calculations much faster than DFT calculations, and provides an easier way
55 to predict the properties of bigger and less symmetric heterostructures. Since we
56 have some experience in using the QP model^{54–56} we studied those papers in de-
57 tails and noticed that a term involving effective charges was neglected/omitted in
58 the definition of polarization that only used the effective dipoles, as in the case of
59 covalent materials such as e.g. graphene. Furthermore, the enforcement of charge
60 conservation was also not implemented, meaning that charges could flow in or
61 out of the materials without any constraint, which can conflict with the fact that
62 an insulating substrate (Polydimethylsiloxane (PDMS), Au, Al₂O₃)^{57,58} was used

63 to obtain the out-of-plane effective flexoelectricity coefficient of monolayer MoS₂,
64 by using an equation for converse flexoelectricity to link the out-of-plane effective
65 piezoelectric coefficient measured by piezoresponse force microscopy and the flexo-
66 electric coefficient to be determined^{57,58}. We also note that in-plane flexoelectric
67 coefficients μ_{1111} or μ_{2222} for such 2D materials have not yet been experimentally
68 obtained, since it has been difficult to isolate the relative contributions of piezo-
69 electricity and flexoelectricity to the resulting polarization.

70 In this work, we computed the in-plane flexoelectric coefficients μ_{1111} , μ_{2222} ,
71 transverse flexoelectric coefficient μ_{3311} and out-of-plane flexoelectric coefficient
72 μ_{3333} for monolayer MoS₂ using the charge-dipole model⁵⁹ with radial Gaussian
73 regularization^{54,56,60-63} enforcing charge conservation with a Lagrange multiplier
74 and adding an ionic charge term in the definition of polarization. The significance
75 of the missing charge term is estimated in the computation of μ_{3333} , by compar-
76 ison with the simulation paper of Javvaji et al.⁵³ and the experimental papers
77 of Brennan et al.^{57,58}. Our calculations illustrate that the results for this flexo-
78 electric coefficient computed with the improved definition of polarization agree in
79 magnitude with experimental measurements, with the possible reason causing the
80 discrepancy in sign discussed. Moreover, two critical factors capable of affecting
81 the sign of flexoelectric coefficient are fully elucidated while μ_{3311} is computed.
82 Additionally, μ_{1111} and μ_{2222} are calculated by using an in-plane displacement field
83 that effectively eliminates the piezoelectric contribution to the polarization.

84 This paper is organized as follows. In Sec.II we describe the Gaussian reg-
85 ularized charge-dipole model, our bending simulation set-ups and the computa-
86 tional methodology for the computation of the strain gradient. The computation
87 of in-plane flexoelectric coefficient μ_{1111} , μ_{2222} , transverse flexoelectric coefficient
88 μ_{3311} and out-of-plane flexoelectric coefficient μ_{3333} are presented and discussed in
89 Sec.III. Section IV concludes our findings.

90 II. METHODS

91 A. Principle of the method used to compute flexoelectricity

92 coefficients

As written in the introduction, the direct flexoelectric effect describes the fact that a strain gradient in a material will cause an (additional) electric polarization of the material, because of the inhomogeneous distribution of positive and negative charge centers caused by the inhomogeneous deformation. Polarization being a vector described by a vector (first order tensor) and strain gradient a third order tensor, the supposedly linear relation between these two quantities is represented by a fourth order flexoelectricity tensor. Various conventions for the signification of the indices, leading to different matrix compressed representations, are used in the literature. We chose the one that puts the index corresponding to the polarization in first place, since we do not make use of the equivalence of the two strain indices:

$$\Delta P_i = \mu_{ijkl} G_{jkl} \quad (1)$$

93 where i, j, k, l are indices labeling the coordinates x, y, z or $1, 2, 3$. The Einstein
94 implied summation convention for repeated indices is used.

95 Our goal is to compute values for these μ_{ijkl} coefficients. For that purpose we
96 will use an inverse effect: when submitted to an external electric field, a dielectric
97 material tends to deform so as to align its global dielectric polarization vector with
98 the external field. Hence, we use various symmetric field configurations designed
99 to deform inhomogeneously a MoS₂ monolayer, while not changing the global po-
100 larization contributions due to the dielectric susceptibility of the material or its
101 piezoelectric properties. Then, we compute both the global polarization and the
102 global strain gradient of the deformed structure and fit the (hopefully linear) re-
103 lation between these two quantities to find the μ coefficients.

104 We shall therefore describe now, how we compute the global polarization and

105 strain gradient in the monolayer.

106 **B. Description of the charge dipole model used to compute the**
 107 **polarization of a monolayer MoS₂ subjected to an external electric field**

We start with the regularized charge-dipole (QP) model^{54,56,60–63}, in which each atom of a MoS₂ nanoribbon is described by the combination of an effective charge and a dipole with radial Gaussian distributions, plus an effective electronegativity. The total electrostatic energy E_{elec} associated with those effective charges $\{q_\alpha\}$ and dipoles $\{\mathbf{p}_\alpha\}$ located at the atomic positions $\{\mathbf{r}_\alpha\}$ (with $\alpha = 1, \dots, N$), in the presence of an external electric field \mathbf{E}_{ext} is given by:

$$E_{elec} = \sum_{\alpha=1}^N q_\alpha(\chi_\alpha + V_{ext,\alpha}) - \sum_{\alpha=1}^N \mathbf{p}_\alpha \cdot \mathbf{E}_{ext} + \frac{1}{2} \sum_{\alpha=1}^N \sum_{\beta=1}^N q_\alpha T_{q-q}^{\alpha,\beta} q_\beta - \sum_{\alpha=1}^N \sum_{\beta=1}^N \mathbf{p}_\alpha \cdot \mathbf{T}_{p-q}^{\alpha,\beta} q_\beta - \frac{1}{2} \sum_{\alpha=1}^N \sum_{\beta=1}^N \mathbf{p}_\alpha \cdot \mathbf{T}_{p-p}^{\alpha,\beta} \cdot \mathbf{p}_\beta \quad (2)$$

where N stands for the number of atoms in the structure considered and χ_α is the electronegativity of the atom α , once inserted in the molecule. $V_{ext,\alpha}$ is the electrostatic potential at \mathbf{r}_α corresponding to the external electric field, which can be expressed as $-\mathbf{E}_{ext} \cdot \mathbf{r}_\alpha$ in the case of a uniform external field. T_{q-q} , \mathbf{T}_{p-q} and \mathbf{T}_{p-p} are interaction tensors between effective point charges or dipoles in vacuum (see equation 3), which have been convoluted with one radial Gaussian distribution per atom, of the form $\pi^{3/2} R_\alpha^3 \exp(-|\mathbf{r} - \mathbf{r}_\alpha|^2 / R_\alpha^2)$. This allows to take into account approximately the extension of the electronic clouds, and prevents the occurrence of divergence problems, i.e. polarization catastrophes, that can occur in simulations when two atoms are so close to each other that the approximation of an interaction between point charges or dipoles is not a good approximation

any more.^{60-62,64,65}

$$\left\{ \begin{array}{l} T_{q-q}^{\alpha\beta} = \frac{1}{4\pi\epsilon_0 r_{\alpha\beta}} \operatorname{erf}\left(\frac{r_{\alpha\beta}}{\sqrt{R_\alpha^2 + R_\beta^2}}\right) \\ \mathbf{T}_{p-q}^{\alpha\beta} = -\nabla_{\mathbf{r}_\alpha} T_{q-q}^{\alpha\beta} = -\frac{1}{4\pi\epsilon_0} \frac{r_{\alpha\beta}}{r_{\alpha\beta}^3} \left[\operatorname{erf}\left(\frac{r_{\alpha\beta}}{\sqrt{R_\alpha^2 + R_\beta^2}}\right) - \frac{2}{\sqrt{\pi}} \frac{r_{\alpha,\beta}}{\sqrt{R_\alpha^2 + R_\beta^2}} \exp\left(-\frac{r_{\alpha\beta}^2}{R_\alpha^2 + R_\beta^2}\right) \right] \\ \mathbf{T}_{p-p}^{\alpha\beta} = -\nabla_{\mathbf{r}_\beta} \otimes \nabla_{\mathbf{r}_\alpha} T_{q-q}^{\alpha\beta} \\ = \frac{1}{4\pi\epsilon_0} \left\{ \frac{3\mathbf{r}_{\alpha\beta} \otimes \mathbf{r}_{\alpha\beta} - r_{\alpha\beta}^2 \mathbf{I}}{r_{\alpha\beta}^5} \left[\operatorname{erf}\left(\frac{r_{\alpha\beta}}{\sqrt{R_\alpha^2 + R_\beta^2}}\right) - \frac{2}{\sqrt{\pi}} \frac{r_{\alpha,\beta}}{\sqrt{R_\alpha^2 + R_\beta^2}} \exp\left(-\frac{r_{\alpha\beta}^2}{R_\alpha^2 + R_\beta^2}\right) \right] \right. \\ \left. - \frac{4}{\sqrt{\pi}} \frac{\mathbf{r}_{\alpha\beta} \otimes \mathbf{r}_{\alpha\beta}}{r_{\alpha\beta}^2} \frac{1}{(\sqrt{R_\alpha^2 + R_\beta^2})^3} \exp\left(-\frac{r_{\alpha\beta}^2}{R_\alpha^2 + R_\beta^2}\right) \right\} \end{array} \right. \quad \forall \alpha \neq \beta \quad (3)$$

where $\mathbf{r}_{\alpha\beta} = \mathbf{r}_\beta - \mathbf{r}_\alpha$ is the vector pointing from α^{th} atom to β^{th} atom. R_α and R_β are the characteristic widths of Gaussian charge distributions for atom type α and β respectively. In the limit $\mathbf{r}_\alpha = \mathbf{r}_\beta$, the expressions of the various $T^{\alpha,\beta}$ interaction tensors in equation 3 converge to finite values (Eq. 4) related to the self-energy for each atom (atomic 'capacitance' or chemical hardness and polarizability).

$$\left\{ \begin{array}{l} q_\alpha T_{q-q}^{\alpha,\alpha} q_\alpha = \frac{q_\alpha^2}{4\pi\epsilon_0} \frac{\sqrt{2/\pi}}{R_\alpha} \\ \mathbf{p}_\alpha \cdot \mathbf{T}_{p-q}^{\alpha,\alpha} q_\alpha = 0 \\ \mathbf{p}_\alpha \cdot \mathbf{T}_{p-p}^{\alpha,\alpha} \cdot \mathbf{p}_\alpha = -\frac{p_\alpha^2}{4\pi\epsilon_0} \frac{\sqrt{2/\pi}}{3R_\alpha^3}. \end{array} \right. \quad (4)$$

108 Our version of the QP model for MoS₂ possesses 8 parameters: 2 (χ and R)
109 per kind of atoms by 4 kinds: Mo and S 'bulk' + Mo and S 'edge'. Details on
110 this parameterization, by comparison with DFT data, are given in our previous
111 work.⁵⁶

The charges and dipoles at electrostatic equilibrium are then determined by minimizing the electrostatic energy (Eq. 2) using a Lagrange multiplier λ to enforce charge conservation in the nanoribbon:

$$f = E_{elec} + \lambda \left(\sum_{\alpha=1}^N q_\alpha - Q_{tot} \right) \quad (5)$$

112 This Lagrange multiplier can be physically interpreted as the chemical potential
113 of the molecule.⁶¹ This enforcement of charge conservation within the framework

114 of QP model is quite essential since it ensures that charges stay in the material
115 in order to mimic the conditions of experimental measurements.⁵⁸ Requiring the
116 derivative of function $f(q, \mathbf{p}, \lambda)$ with respect to $q_\alpha, p_{x,\alpha}, p_{y,\alpha}, p_{z,\alpha}$ and λ to be zero
117 will give a system of $4N + 1$ linear equations for determining the $4N + 1$ scalar
118 unknowns ($q_\alpha, p_{x,\alpha}, p_{y,\alpha}, p_{z,\alpha}$ and λ). These linear equations may be written in a
119 matrix form:

$$\begin{bmatrix} T_{q-q} & \mathbf{T}_{p-q}^t & 1 \\ \mathbf{T}_{p-q} & \mathbf{T}_{p-p} & 0 \\ 1 & 0 & 0 \end{bmatrix} \begin{bmatrix} q \\ \mathbf{p} \\ \lambda \end{bmatrix} = \begin{bmatrix} -(\chi + V_{ext}) \\ -\mathbf{E}_{ext} \\ Q_{tot} \end{bmatrix} \quad (6)$$

where T_{q-q} is a block matrix with N rows and N columns. \mathbf{T}_{p-p} is a block matrix with $3N$ rows and $3N$ columns. \mathbf{T}_{p-q} is a block matrix with $3N$ rows and N columns. \mathbf{T}_{p-q}^t is the transpose of \mathbf{T}_{p-q} . Similarly, blocks q and $-(\chi + V_{ext})$ have N rows and 1 column, while blocks \mathbf{p} and $-\mathbf{E}_{ext}$ have $3N$ rows and 1 column. We note that the solution can be written in two parts as:

$$\begin{bmatrix} q \\ \mathbf{p} \\ \lambda \end{bmatrix} = \begin{bmatrix} T_{q-q} & \mathbf{T}_{p-q}^t & 1 \\ \mathbf{T}_{p-q} & \mathbf{T}_{p-p} & 0 \\ 1 & 0 & 0 \end{bmatrix}^{-1} \begin{bmatrix} -\chi \\ 0 \\ Q_{tot} \end{bmatrix} + \begin{bmatrix} T_{q-q} & \mathbf{T}_{p-q}^t & 1 \\ \mathbf{T}_{p-q} & \mathbf{T}_{p-p} & 0 \\ 1 & 0 & 0 \end{bmatrix}^{-1} \begin{bmatrix} -V_{ext} \\ -\mathbf{E}_{ext} \\ 0 \end{bmatrix} \quad (7)$$

where the first term on the right side corresponds to intrinsic charges q_α^0 and dipoles \mathbf{p}_α^0 , i.e. charges and dipoles in the absence of any external electric field, that can however vary due to a mechanical deformation. The electronegativities χ_α uniquely determine these intrinsic charges and dipoles (given the atomic positions), independently from any external electric field \mathbf{E}_{ext} or potential V_{ext} . For our calculations, the total charge of the nanoribbon (Q_{tot}) is set to be zero because of the fact that flexoelectricity is supposed to be an intrinsic property, therefore requiring no extra charge to appear. The second term on the right side corresponds to effective additional charges (q_α^{ind}) and dipoles (\mathbf{p}_α^{ind}) generated by the external

electric field and potential). This can be summarized under the form:

$$\left\{ \begin{array}{l} p_x = \sum_{\alpha=1}^N (p_{x,\alpha}^0 + p_{x,\alpha}^{ind}) \\ p_y = \sum_{\alpha=1}^N (p_{y,\alpha}^0 + p_{y,\alpha}^{ind}) \\ p_z = \sum_{\alpha=1}^N (p_{z,\alpha}^0 + p_{z,\alpha}^{ind}) \\ q = \sum_{\alpha=1}^N (q_{\alpha}^0 + q_{\alpha}^{ind}) \end{array} \right. \quad (8)$$

In terms of the calculated dipoles \mathbf{p} and charges q , the global polarization \mathbf{P} for MoS₂ nanoribbon is defined as⁵⁹:

$$\mathbf{P} = \frac{\sum_{\alpha=1}^N (q_{\alpha} \mathbf{r}_{\alpha} + \mathbf{p}_{\alpha})}{V} \quad (9)$$

120 in which V is the volume of MoS₂ nanoribbon. A thickness of 6.5 Å is used in
 121 computing V .⁶⁶ More information on the charge dipole model for MoS₂ can be
 122 found in our previous work⁵⁶. Note that since MoS₂ is not ferroelectric, the total
 123 contribution to polarization of the q_{α}^0 and \mathbf{p}_{α}^0 is zero (verified numerically), so that
 124 Eq. 9 could be rewritten by taking into account the induced charges and dipoles
 125 only.

126 In order to compare with some DFT results or remove edge effects, periodic
 127 boundary conditions can be applied in the QP model by adding the contributions
 128 of periodic images in the interaction tensors, i.e. adding contributions obtained by
 129 replacing $r_{\alpha\beta}$ in Eq.3 with $r_{\alpha\beta} + L * p$ ($p \in [-k, k]$), with L denoting the periodic
 130 length in a given direction and k being a very large integer. We verified that
 131 setting $k = 100$ in our calculation is already sufficiently large to reach convergence
 132 in the computation of in-plane flexoelectric coefficients μ_{1111} , μ_{2222} and out-of-plane
 133 flexoelectric coefficient μ_{3333} , thus eliminating edge effects.

134 C. Calculation of flexoelectricity coefficients

135 We illustrate the method we use to compute the flexoelectric coefficients on the
136 special case of the determination of μ_{3311} .

137 1. *potential energy functional used for the 'structure' part*

138 The key of the molecular simulations is actually the interatomic potential, which
139 is applied to describe the interaction among atoms. For single-layer MoS₂, the
140 Stillinger-Weber many-body potential (E_{SW}) as parameterized by Wen et al⁶⁷ was
141 very recently proven to be robust through a quantitative systematic comparison of
142 structural and mechanical properties, as well as phonon dispersion for single-layer
143 MoS₂ using density functional theory (DFT) and molecular statics calculations.⁶⁸
144 We therefore used this parameterization of the SW potential (E_{SW}) in our simula-
145 tions, and found it very stable. Its analytical form and the values of the parameters
146 are recalled in [Supplementary material](#). The various MoS₂ nanoribbons we use in
147 our simulations are thus initially relaxed by minimizing E_{SW} . This gives the un-
148 deformed configuration mentioned in the previous subsection.

149 To compute the deformed configurations, we removed the interactions between
150 intrinsic charges and dipoles in E_{elec} , since they are already included in E_{SW} .
151 We also neglected the total contribution of the interactions between intrinsic and
152 induced charges and dipoles to keep only the total contributions of the interactions
153 between charges and dipoles induced by the external field and potential (which we
154 name E'_{elec}).

155 2. *Initial conditions for the calculation of μ_{3311}*

156 In order to compute μ_{3311} , a \searrow/\swarrow -like external electric field \mathbf{E}_{ext} , with both
157 directions of \mathbf{E}_{ext} in the x - z plane, is applied to the MoS₂ nanoribbon, keeping the

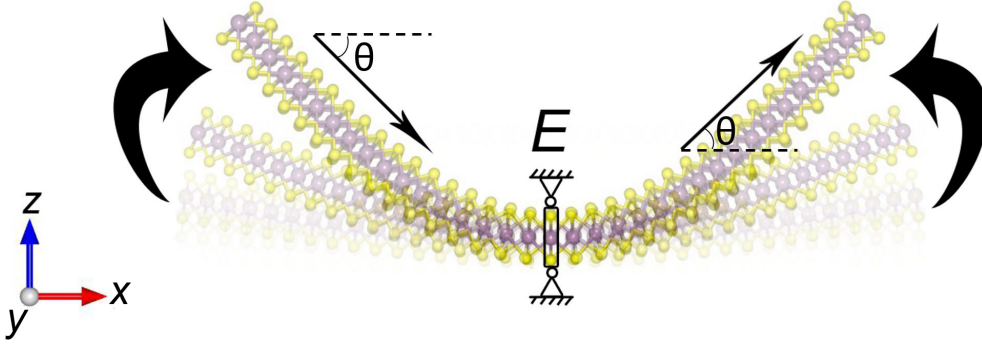


FIG. 1. Schematic of bending simulation for MoS₂ nanoribbon subjected to an external electric field. The left and right parts of the MoS₂ sheet are submitted to an electric field in the bottom-right and top-right direction, respectively. The external electric field \mathbf{E} is represented by the arrows. θ is the angle with the $+x$ direction.

158 middle row of atoms fixed (as if it were attached to a virtual fixed object). This
 159 field generates a bending deformation of the nanoribbon because of the inverse
 160 flexoelectric effect, as seen in Fig 1. The conjugate gradient algorithm is then
 161 used to minimize the energy function $E_{tot} = E_{SW} + E'_{elec}$ which now includes
 162 the interactions with the external field and potential and the contributions of the
 163 effective induced charges and dipoles. The energy optimization simulation then
 164 makes the MoS₂ flake bend towards the direction of the applied electric field by
 165 adjusting the positions of the atoms until the computed average force is less than
 166 0.00004 eV/Å. Note that all these simulations are done with a FORTRAN code
 167 that has been continuously developed in the group for years.

168 The mechanism of electrostatic bending of MoS₂ flake is depicted in Figure
 169 1 of Supplementary material. We can see that negative and positive charges are
 170 shifted to opposite directions due to the non-zero transversal electric field (positive
 171 charges move to upper left and negative ones move to top right of the MoS₂ flake).
 172 The interaction between the electric field generated by the induced charges and
 173 the external electric field produces two torques with opposite direction, termed τ_1

174 and τ_2 , which may be expressed as $q\mathbf{r} \times \mathbf{E}_{ext}$, making the two sides of the MoS₂
 175 flake respectively bend towards the direction of the external electric field with the
 176 fixed atoms as the rotation axis, while giving a zero total polarization along the
 177 vertical axis.

178 3. Calculation of μ_{3311}

Contributions to the polarization of a given dielectric material submitted to an external electric field may come from piezoelectricity, flexoelectricity and electric susceptibility. In the simulations defined in the previous subsection, piezoelectricity may not be taken into account due to the symmetric bending deformation⁵². This makes the total induced polarization due to the first order deformation gradient become zero. Additionally, one can find the total external electric field along the out-of-plane is also zero. Hence, the out-of-plane polarization equal to the product of the susceptibility and the electric field should be removed as well. The remaining flexoelectric part of the out-of-plane polarization P_3 can be written as:

$$P_3 = \sum_{j=1}^3 \sum_{k=1}^3 \sum_{l=1}^3 \mu_{3jkl} G_{jkl} \quad (10)$$

with μ_{3jkl} standing for flexoelectric tensor components. With the setup defined in the previous section, this can be approximated by:

$$P_3 = \mu_{3311} G_{311} \quad (11)$$

179 Hence μ_{3311} can be determined as the slope of the supposedly linear relation be-
 180 tween P_3 and G_{311} . Details on the computing method for determining strain
 181 gradient can be found in Supplementary material.

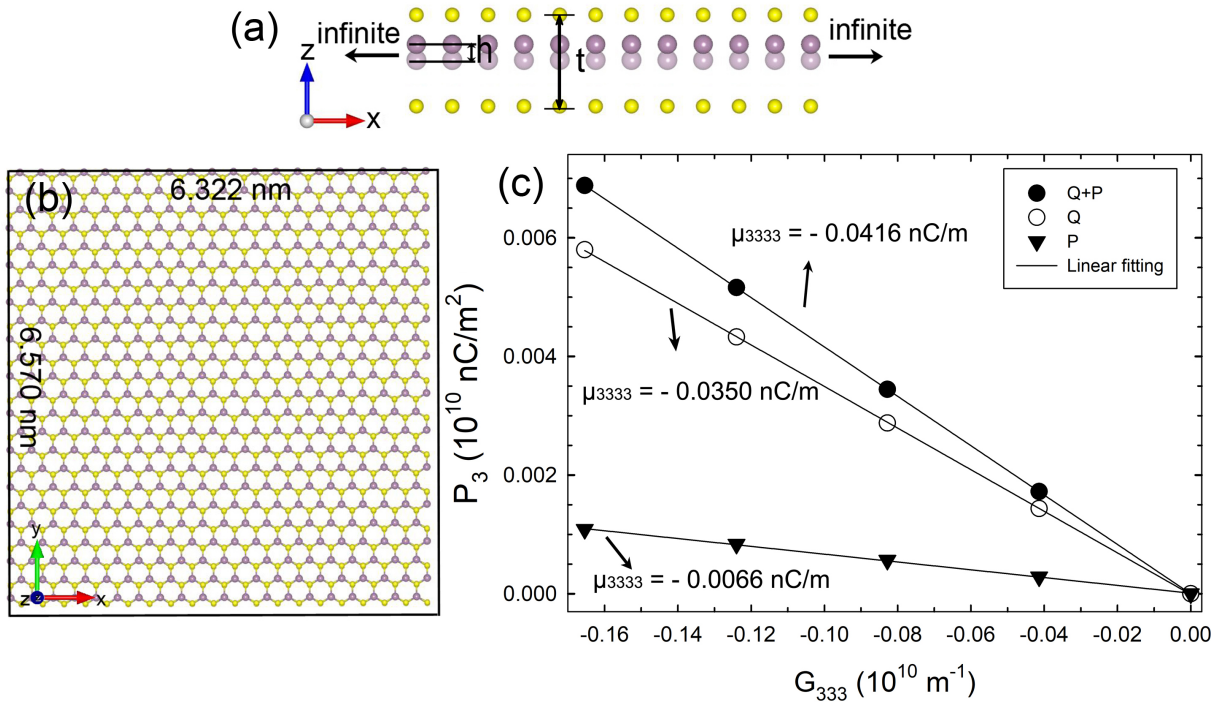


FIG. 2. (a) Schematic diagram of creation of strain gradient G_{333} inside monolayer MoS₂. h and t stand for the small upward shift for a layer of molybdenum atom and the geometric thickness of monolayer MoS₂, respectively. (b) Basic unit for periodic monolayer MoS₂, with length and width of basic unit being 6.570 nm and 6.322 nm, respectively. (c) Variation of polarization P_3 with strain gradient G_{333} for monolayer MoS₂.

182 III. RESULTS AND DISCUSSION

183 In this section, we discuss the results we got for the computation of the in-
 184 plane flexoelectric coefficients μ_{1111} , μ_{2222} , the transverse flexoelectric coefficient
 185 μ_{3311} and the out-of-plane coefficient μ_{3333} . The parameters for E_{SW} and QP
 186 model used in this work were initially validated through calculation of the in-
 187 plane piezoelectric constant e_{222} for an MoS₂ monolayer. We found a value of the
 188 same order of magnitude as the corresponding experimental result (more details

189 are given in Supplementary material).

190 A. Out-of-plane flexoelectric coefficient μ_{3333}

191 As can be seen on Fig.2a, for this calculation, the layer of molybdenum atoms
192 is shifted a small distance h to the positive direction of z axis to generate a strain
193 gradient only along the out-of-plane (z) direction. In this case, the unique strain
194 gradient that does exist is G_{333} and the expression for computing μ_{3333} can be
195 written as $\mu_{3333} = \frac{\partial P_3}{\partial G_{333}}$. The geometric thickness of monolayer MoS₂ is t . With
196 both h and t , the strain gradient G_{333} can be computed as $-\frac{8h}{t^2}$, which may be
197 derived by: $G_{333} = \frac{d^2 u_z(0)}{dz^2} \approx \frac{u_z(-\frac{t}{2}) + u_z(\frac{t}{2}) - 2u_z(0)}{(t/2)^2} = \frac{0+0-2h}{(t/2)^2} = -\frac{8h}{t^2}$, with $u_z(\frac{t}{2})$,
198 $u_z(-\frac{t}{2})$ and $u_z(0)$ representing the displacement of atoms for top sulfur layer,
199 bottom sulfur layer and molybdenum layer, respectively. In this calculation, we
200 enforce periodic boundary conditions to eliminate edge effects that can be quite
201 important in such a setup. As can be seen on Fig.2b, we use a MoS₂ flake with a
202 width of 6.164 nm and a length of 6.388 nm as supercell, which gives periods along
203 x and y direction of 6.322 nm and 6.570 nm, respectively. Bond length between
204 Mo and S is set as 2.39763 Å in the presence of periodic boundary conditions.
205 On Fig.2c, we plot the polarization P_3 as a function of G_{333} , in order to obtain
206 the flexoelectric coefficient μ_{3333} of 2D MoS₂. Three different ways to compute
207 the polarization are used (using $q_\alpha \mathbf{r}_\alpha$ only, using \mathbf{p}_α only or using both terms in
208 Eq.9, with charges and dipoles computed using the QP scheme in the three cases).
209 The units of polarization P_3 and strain gradient G_{333} are converted from e/Å²
210 and Å⁻¹ to 10¹⁰ nC/m² and 10¹⁰ m⁻¹ respectively, so as to readily obtain μ_{3333} in
211 nC/m from the slope of the fitted straight line. We compare μ_{3333} computed under
212 the various definitions of polarization with that obtained from the experimental
213 measurements conducted by Brennan et al in 2017 and 2020^{57,58}, respectively, as
214 shown in Table I.

TABLE I. Comparison between out-of-plane flexoelectric coefficients μ_{3333} obtained by charge-dipole model and experimental measurements. The two different contributions to the polarization coming from charges alone or dipoles alone are considered separately then together for the computation of μ_{3333} by the charge-dipole model.

Ref.	μ_{3333} (nC/m)	Definition of polarization
present work	-0.0416	$P_3 = \frac{\sum_{\alpha=1}^N (q_{\alpha} r_{3,\alpha} + p_{3,\alpha})}{V}$
present work	-0.0350	$P_3 = \frac{\sum_{\alpha=1}^N q_{\alpha} r_{3,\alpha}}{V}$
present work	-0.0066	$P_3 = \frac{\sum_{\alpha=1}^N p_{3,\alpha}}{V}$
Brennan et al (2017) ⁵⁷	0.08 or 0.12	————
Brennan et al (2020) ⁵⁸	0.065	————

215 It can be seen that the result for μ_{3333} computed when the charge term is
216 included in the definition of polarization will be comparatively closer to the exper-
217 imental result in absolute value whereas μ_{3333} computed with the dipole term only
218 considered is of the same order of magnitude but much smaller than the experi-
219 mental value. This manifests that the charge term, omitted/neglected in Ref.⁵²,
220 cannot be neglected for the calculation of polarization for MoS₂. We do not take
221 into account the discrepancy in sign between our computed results and the results
222 of the Piezoresponse Force Microscopy (PFM) measurements of Brennan et al.,
223 since we believe that it is due to a problem of different definition for the algebraic
224 (or not) radius of curvature. This is reflected in another experimental measure-
225 ments of out-of-plane flexoelectric coefficient μ_{3333} for few-layers MoS₂ with PFM,
226 very recently conducted by Hirakata et al⁶⁹. In their work, the sign of the out-
227 of-plane flexoelectric coefficient is measured to be negative, though they quote a
228 positive number. Indeed, using their Eq. 9, one can get $\mu_{3333} = \mu_{39} = -c_{33}\epsilon_3/\frac{\partial E_3}{\partial x_3}$.

229 Since c_{33} , ϵ_3 and $\frac{\partial E_3}{\partial x_3}$ (see their Figure 11) are all positive, their μ_{3333} is in fact
230 negative.⁶⁹

231 Other problems could arise because the MoS₂ samples used in the PFM exper-
232 iments might not be as perfect as that used in our calculation. Indeed, intrinsic
233 atomic defects have been observed in the CVD-grown monolayer MoS₂ using near-
234 field photoluminescence imaging⁷⁰. These defects could give rise to very localized
235 strain gradients and therefore to noticeable additional polarization due to flexo-
236 electricity, since monolayer MoS₂ is sensitive to any tiny deformation along vertical
237 direction (z) due to its atomically thin thickness. Furthermore, the possibly exist-
238 ing interfacial contamination between substrate and MoS₂ sample and the other
239 uncertainties relevant to the measurements could be another cause of discrepancy
240 between our theoretical results and the experimental ones. It would be useful if
241 these (difficult) experiments could be repeated many times, so as to reduce the
242 large uncertainties on the experimental results, but we feel that our present results
243 for μ_{3333} of a MoS₂ monolayer, agree well enough with experiment, to encourage
244 us to compute other flexoelectric coefficients for MoS₂ monolayer, for which we do
245 not have experimental data to compare with.

246 B. Transverse flexoelectric coefficient μ_{3311}

247 The bending simulation described in the 'Methods' section is employed to com-
248 pute the transverse flexoelectric coefficient μ_{3311} of MoS₂. Since the visible dis-
249 placements are mostly along z direction, the strain gradient enabling polarization
250 to be nonzero is principally G_{311} . Hence, μ_{3311} may be approximately expressed
251 as $\mu_{3311} = \frac{\partial P_3}{\partial G_{311}}$. Fig.3a presents the variations of the out-of-plane polarization P_3
252 for a MoS₂ flake bent along (x) zigzag direction with respect to the strain gradient
253 G_{311} . One can notice that the intercept of the linear-fitting straight line is almost
254 zero, meaning that the nonzero polarization is mainly caused by G_{311} .

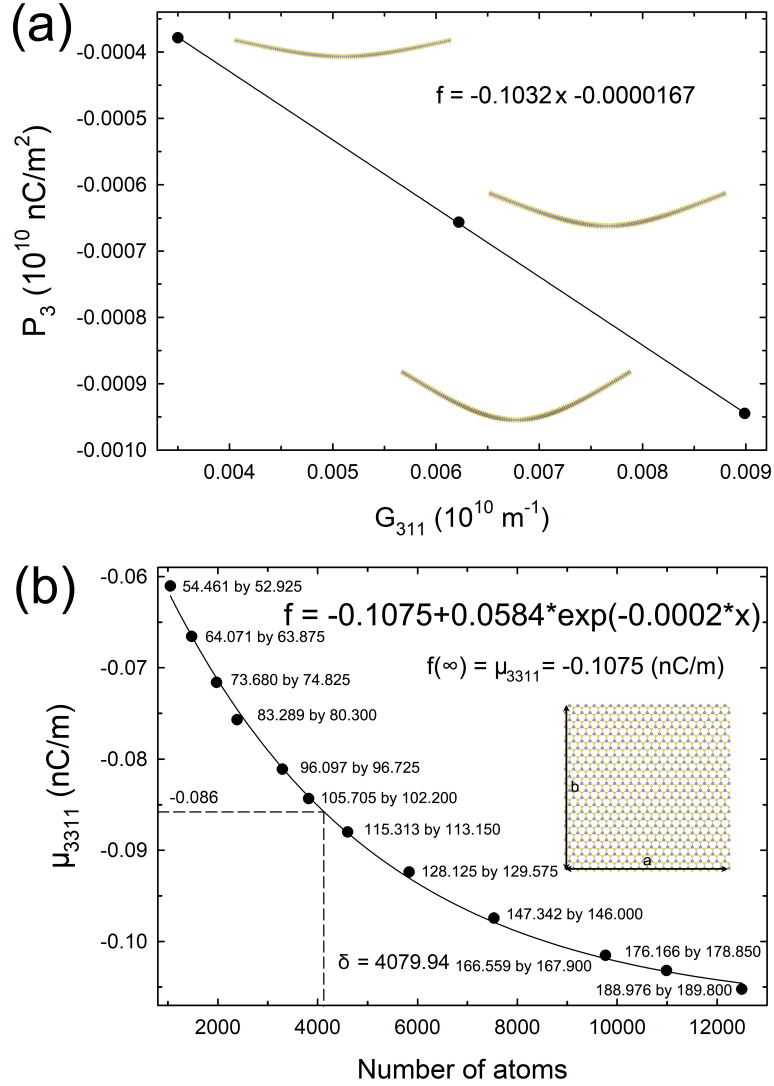


FIG. 3. (a) Variation of P_3 with strain gradient G_{311} . The magnitude of the electric fields imposed to the MoS₂ monolayer for bending simulation are 0.0424 V/Å, 0.0566 V/Å, 0.0707 V/Å, respectively. (b) Transverse flexoelectric coefficient μ_{3311} vs number of atoms. An exponential function is used to describe the tendency to convergence. The lengths a and b of the sides the of MoS₂ flakes are marked next to each computed μ_{3311} . The first and second number for the size of MoS₂ flake corresponds to a and b , respectively. The unit of a and b is Å. δ denotes characteristic length of exponential function. The angle between the electric field and the positive direction of the x-axis is set to 45 degrees.

255 Contrarily to what we did for the computation of μ_{3333} , periodic boundary
 256 conditions cannot be exerted in the bending simulation because bending of material
 257 submitted to the external electric field will break the periodicity of the lattice itself.
 258 We therefore studied the effect of the size of the MoS₂ flake, on the computed
 259 flexoelectric coefficient. Fig.3b is plotted to present the variation of transverse
 260 flexoelectric coefficient μ_{3311} with the increasing number of atoms. It can be seen
 261 that the value of μ_{3311} scales non-linearly down with the number of atoms. The
 262 larger the number of atoms, the more obvious the trend of curve convergence. To
 263 obtain a converged value, data is fitted with an exponential function. With the
 264 number of atoms increasing, the transverse flexoelectric coefficient μ_{3311} converges
 265 to -0.1075 nC/m, comparable to that for phosphorene⁴⁷ and boron nitride sheet⁴⁸.
 266 A comparison is made between μ_{3311} computed with QP model and that obtained
 267 by DFT-based first principle calculation by Shashikant et al⁵¹, as listed in Table II.
 268 It can be seen that our computed result for μ_{3311} agrees much better in absolute
 269 value with that obtained from DFT calculations than the one computed by Zhuang
 270 et al.⁵², signifying that the computation of transverse flexoelectric coefficient of
 271 MoS₂ can be well captured by the QP model, if the proper definition for the
 272 polarization is used. **Note that the radial polarization \mathbf{p}_r defined in reference⁵¹**
 273 **and⁷¹ to compute μ_{3311} can be considered equivalent to the p_z used in our work,**
 274 **since it is always locally perpendicular to the 2D material.** We will now turn again
 275 to the question of the sign of the flexoelectric coefficients.

277 Understanding the reason causing the discrepancy in the sign of flexoelectric
 278 coefficients is essential because the direction of the electric polarization induced by
 279 flexoelectricity is of significance for sensors and energy harvesters. We will study
 280 successively the sign of the polarization and the strain gradient.

281 Concerning polarization, we separate two distinct contributions: one due to
 282 the deformation of the lattice and the other one due to charge transfer between
 283 the inner and outer layers during bending. For that purpose we first compute

TABLE II. Comparison between transverse flexoelectric coefficient μ_{3311} obtained by charge dipole model and theoretical computation.

Ref.	μ_{3311} (nC/m)
present work	-0.1075
Shashikant et al ⁵¹	0.14
Zhuang et al ⁵²	0.032

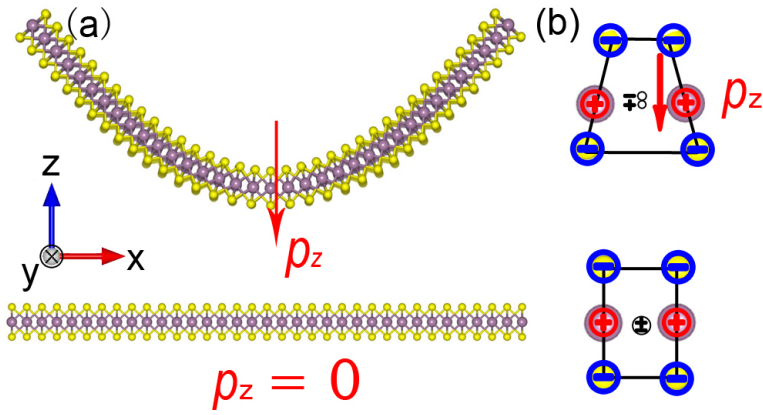


FIG. 4. Origin of flexoelectric effect in bending deformation. (a) Under bending deformation, the direction of induced dipole moment points to $-z$ direction. For an undeformed MoS_2 flake, the total dipole moment along the direction normal to the surface of MoS_2 is zero. (b) Separation of the centers (in black) of positive (in red) and negative charges (in blue) due to bending deformation.

284 the relaxed positions of a MoS_2 flake deformed under the action of an electric
 285 field, using the QP model (Fig.4a). Then we compute the polarization for that
 286 bent MoS_2 flake, for an hypothetical case where the charges of the sulfur atoms
 287 would be the same in the upper and lower layers. In that hypothetical case, the
 288 computation gives a polarization in the negative direction of z axis, whereas in the
 289 undeformed MoS_2 flake, the total dipole moment along the out-of-plane direction

290 is always zero due to the fact that the molybdenum atomic layer is equidistantly
 291 sandwiched between two layers of sulfur atoms. Fig.4b illustrates this phenomenon
 292 with the case of the two rows of atoms nearest to the symmetry plane of the
 293 deformed flake: the molybdenum cations are repelled away from the inner part
 294 of the bend (which is its denser part). The consequence is that, while the charge
 295 center of the sulfur anions stays half way between the two layers, the charge center
 296 of the molybdenum is lower which results in a polarization pointing downwards
 297 (hence a negative contribution to μ_{3311} since G_{311} is positive in that case).

298 However, the above effect is not enough to fully account for the polarization
 299 since we artificially used identical charges for the sulfur atoms. In reality, since
 300 the overlapping of the electronic clouds of two nearby ions change during bending,
 301 partial charges can be transferred from one sulfur layer to the other. In order to
 302 understand that second contribution to the polarization, two representative areas
 303 of the same deformed MoS₂ flake, named A and B, are considered in Fig.5a. The
 304 average charge for the sulfur atoms in the upper and lower layers, calculated by
 305 averaging net charges obtained by the QP model along y direction perpendicular
 306 to the figure, are $-0.776 e$ and $-0.803 e$, respectively. Therefore the atoms of the
 307 lower sulfur layer appear to be more negative than those of the upper layer. This
 308 creates a net dipole moment pointing from the outside to the inside of the curvature
 309 (in the positive direction of z axis in our case). At the B site, the curvature is
 310 much smaller than at the A site and consequently the difference in charges between
 311 sulfur atoms in the upper and lower layer is smaller. In Fig.5b, we plotted the
 312 average charge difference $\Delta q = q_{lower} - q_{upper}$ between sulfur atoms in the lower and
 313 upper layer, as a function of their index along the x coordinate (see numbers on the
 314 molecular picture inside the graph). It can be seen that the absolute value of Δq
 315 decreases with the increasing index of sulfur, which agrees with what we expected
 316 before implementing the computation, since it corresponds to the flexoelectric
 317 effect: if the strain gradient is smaller, then the polarization is smaller (in absolute

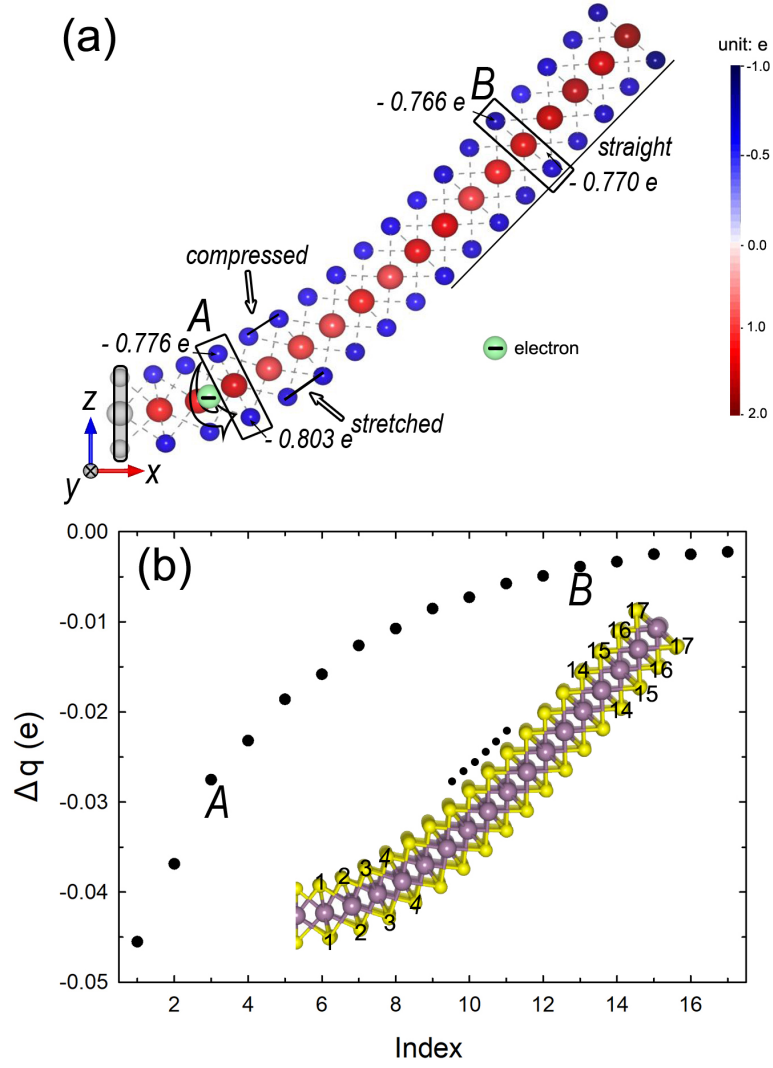


FIG. 5. (a) Charge distribution of a bent MoS₂ subjected to $E_x = E_z = 0.4 \text{ V/\AA}$. A and B are two representative regions for explanation of charges transfer from the upper layer to the lower layer, respectively. (b) Δq vs index. Δq is calculated as the charge of sulfur atoms in the lower layer minus the corresponding quantity for the upper layer. The upper and lower sulfur atoms are numbered by increasing value of z . Only the right portion of the bent MoS₂ is shown here.

318 value). Hence, we have two contributions in opposite directions: a downward
 319 electric dipole moment due to bending of the lattice and an upward electric dipole
 320 moment due to charge transfer. In the case of MoS₂, our computations show
 321 that polarization caused by bending deformation of lattice (which tends to give
 322 a negative flexoelectric coefficient) surpasses that resulting from charge transfer
 323 (which tends to give a positive flexoelectric coefficient). It is worth mentioning
 324 here that a negative μ_{3311} for MoS₂ monolayer has very recently been obtained
 325 using first-principles linear-response theory⁷¹. Very interestingly, it can be found in
 326 their calculations that two contributions coming from the dipolar and the lattice-
 327 mediated response, respectively, to the total polarization response also play a
 328 competing role, the signs of the former and the latter tending to be opposite, as
 329 in our study.

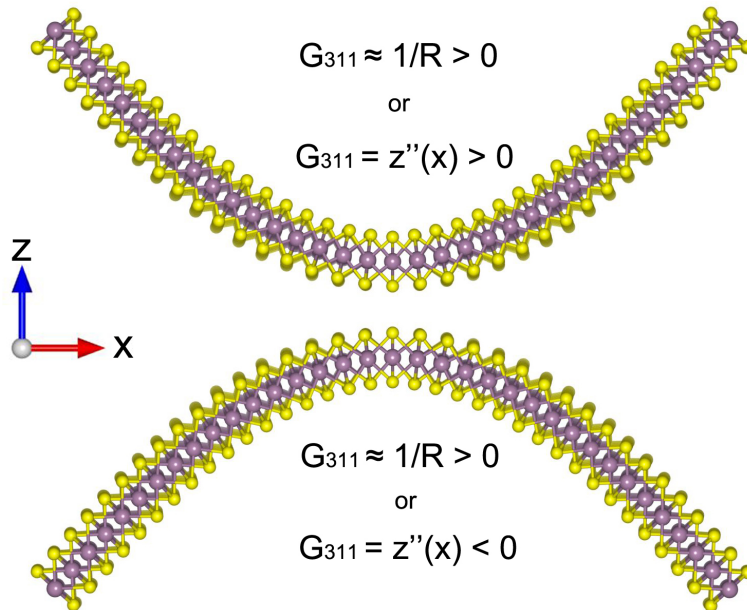


FIG. 6. Illustration of the different definitions for strain gradient G_{311} .

330 We now turn to the sign of the strain gradient. In a review paper, Wang et al⁷²
 331 pointed the discrepancies between definitions and symbols of physical quantities

332 to be one of the reasons for the inconsistency of the reported signs of flexoelectric
333 coefficients. It is often the case for the strain gradient G_{311} . Indeed, on Fig.6
334 we illustrate that the strain gradient, defined as $G_{311} = u_z''(x)$ which can be either
335 positive or negative, is often approximated as the inverse of the radius of curvature.
336 Since, for some authors, the radius of curvature is always positive, G_{311} is always
337 positive for them, regardless of the bending direction of the material. Slightly
338 differently, Kundalwal et al⁴⁸ considered a boron nitride sheet shaped as an upward
339 convex curved arch and defined G_{311} as the absolute value of the inverse of radius
340 of curvature. We note, however, that we used a downward pointing bend (top part
341 of Fig.6 and Fig.4) which gives a positive strain gradient for all these definitions.

342 The previous considerations tentatively explain why flexoelectric coefficients
343 can be either positive or negative, due to a competition between lattice and charge
344 transfer effect, and not always positive as some authors define it by using absolute
345 values inside their definition.

346 C. In-plane flexoelectric coefficient μ_{1111} and μ_{2222}

347 Inspired by the work of Hong et al⁷³, the in-plane flexoelectric coefficients μ_{1111}
348 and μ_{2222} are computed in the present work. Strain gradient G_{111} is created by dis-
349 placing every atoms along x axis, according to a parabolic displacement function
350 $u_x(x)$. Fig.7a is a schematic diagram showing the transverse displacement of atoms
351 for a MoS₂ flake with a bigger (so that it be visible thanks to the two vertical lines)
352 strain gradient imposed along x axis. Fig.7b shows the variation of displacement
353 of atoms along x direction in the case $\Delta d = u_x(x) = 0.01 - 10^{-5}x^2$, strain ϵ_{xx} and
354 strain gradient $\epsilon_{xx,x}$ (G_{111}) as functions of the position along x axis for MoS₂. We
355 can see that the total strain is zero due to the symmetric distribution of displace-
356 ment with respect to $x = 0$. Hence, the polarization due to piezoelectricity can be
357 fully removed from the total polarization, leaving only flexoelectricity. Further-

358 more, μ_{1111} can be expressed as $\mu_{1111} = \frac{\partial P_1}{\partial G_{111}}$ and for a similar simulations with
 359 parabolic displacement along y , $\mu_{2222} = \frac{\partial P_2}{\partial G_{222}}$. The magnitude of strain gradient
 360 for our calculations of μ_{1111} and μ_{2222} ranges from 0 to 0.00004 \AA^{-1} , which is small
 361 enough to neglect any non-linear effect.

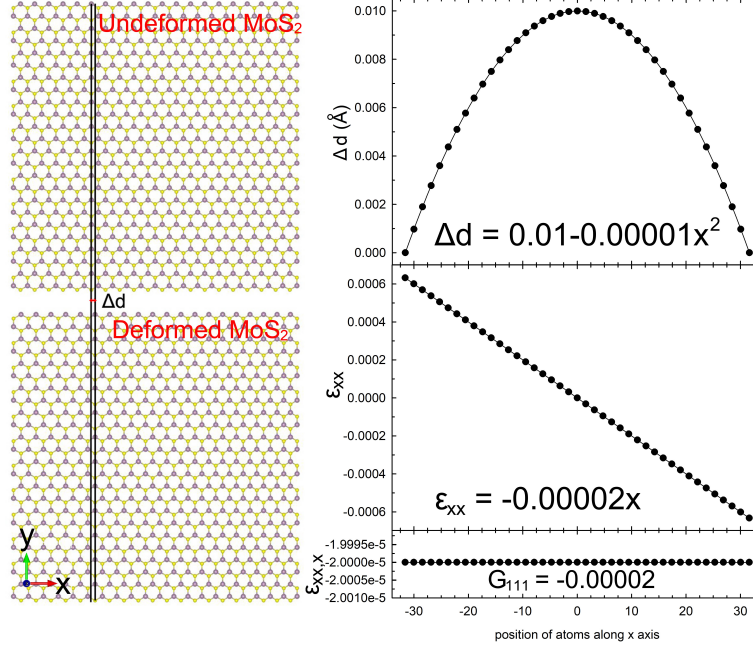


FIG. 7. (a) Applied displacement field along x axis for each atom with Δd denoting the
 difference between the x coordinate of atoms in deformed MoS₂ and that in undeformed
 MoS₂. The two vertical lines are guides to the eye to see the displacements along x
 between the top and bottom sub-figures. (b) Displacement field $\Delta d = u_x(x)$, strain (ϵ_{xx})
 and strain gradient ($\epsilon_{xx,x} = G_{111}$) vs the position along x axis for MoS₂.

362
 363
 364 The dependence of in-plane flexoelectric coefficients μ_{1111} and μ_{2222} on the width
 365 of nanoribbon with infinite lengths is shown in [Figure 4 in Supplementary material](#).
 366 Clearly, the in-plane flexoelectric coefficients increase as the width of nanoribbons
 367 increases (polynomial fits are guides to the eye). The non-convergence behavior
 368 of those flexoelectric coefficients with the increase of the width of the nanoribbons
 369 has been elaborately discussed⁷⁴. Hao et al. reveals through DFT calculations that

370 the flexoelectric coefficients of the 2D Janus TMDs nanoribbons depend strongly
 371 upon their widths. The (slightly) different results for the two orientations are
 372 probably due to edge effects different for armchair and zigzag edges. To completely
 373 eliminate edge effect we use periodic boundary conditions in both directions for the
 374 displacements. In their article,⁷³ Hong et al. computed the in-plane flexoelectric
 375 coefficients of SrTiO₃ using a strain gradient with a cosine form, to be compatible
 376 with the periodic boundary conditions. In our work, strain gradient is a constant
 377 function (see Fig.7b), which is an even simpler case. Fig.8 shows the variations
 378 of polarization P_1 and P_2 with strain gradient G_{111} and G_{222} for those doubly-
 379 periodic setups. The computed flexoelectric coefficients μ_{1111} and μ_{2222} are 0.6872
 380 nC/m and 0.7119 nC/m, respectively. Hence, the in-plane flexoelectric properties
 381 of doubly-infinite MoS₂ are nearly isotropic, i.e. independent of the zigzag or
 382 armchair direction.

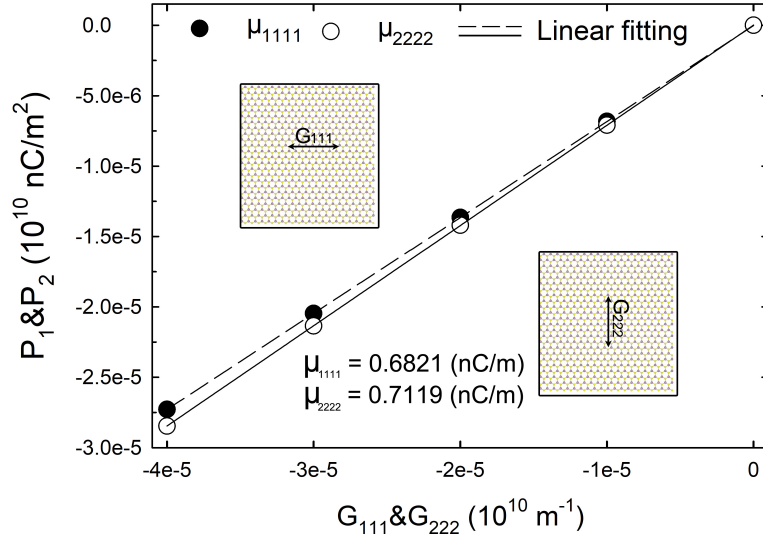


FIG. 8. Variations of polarization P_1 and P_2 with strain gradient G_{111} and G_{222} , respectively. The rectangular frame surrounding the edge of molybdenum disulfide represents the enforcement of periodic boundary conditions in both directions.

383 IV. CONCLUSIONS

384 Employing three different simulation setups, we calculated in-plane flexoelectric
385 coefficients μ_{1111} , μ_{2222} , transverse flexoelectric coefficient μ_{3311} and out of plane
386 flexoelectric coefficient μ_{3333} for monolayer MoS₂ using the charge dipole model and
387 charge conservation. The out-of-plane flexoelectric coefficient μ_{3333} and transverse
388 flexoelectric coefficient μ_{3311} computed by the charge-dipole model are compared
389 with those obtained by experimental measurements and DFT-based first principle
390 calculations, by which good agreement in absolute value can be seen when the
391 charge term is included in the computation of the polarization. We discuss in
392 details possible origins of discrepancy in sign between our calculated flexoelectric
393 coefficient μ_{3311} and other reported results, by showing two opposite effects for the
394 sign of the polarization. Furthermore, we emphasize that comparison of flexoelec-
395 tric coefficients between different computational works requires a careful check for
396 the sign of strain gradient and the way of defining the polarization. Concerning
397 the computed in-plane flexoelectric coefficient μ_{1111} and μ_{2222} are found to be quasi
398 identical, which is consistent with the analysis of symmetry for the flexoelectric
399 coefficient tensor of a 2D continuum.

400 Finally, it is worth pointing out that the computed in-plane flexoelectric coef-
401 ficient is about twenty times greater than out-of-plane flexoelectric coefficient for
402 MoS₂, which can be ascribed to the fact that the net charges induced by in-plane
403 strain gradient between every primitive cells lead to the generation of larger electric
404 dipole moments, whereas the movement of the charge in the out-of-plane direction
405 is restricted due to the finite thickness. Hence, a relatively small polarization is
406 then induced in the out-of-plane direction. **For 2D materials, bending seems to**
407 **be the easiest way to externally generate a big strain gradient at nanoscale, on a**
408 **large area. Therefore, even if in-plane flexoelectric coefficients may play a role in**
409 **some systems, the differences between in-plane, out-of-plane and transverse coef-**
410 **ficients in MoS₂ flakes is not big enough to compensate for the bigger and more**

411 homogeneous strain gradient that can be realized by bending. It is thus important
412 to find 2D materials that optimize the transverse flexoelectric coefficients μ_{3311} for
413 applications in energy harvesting.

414 V. ACKNOWLEDGMENTS

415 This work was supported by the EIPHI Graduate School (contract "ANR-17-
416 EURE-0002") and the Region of Bourgogne Franche-Comté (contract 2018-0054
417 "ACTION μ Mecatru. Computations have been performed on the supercomputer
418 facilities of the Mésocentre de calcul de Franche-Comté.

419 VI. DATA AVAILABILITY

420 The data that support the findings of this study are available from the corre-
421 sponding author upon reasonable request.

422 REFERENCES

- 423 ¹P. V. Yudin and A. K. Tagantsev, "Fundamentals of flexoelectricity in solids,"
424 *Nanotechnology* **24**, 432001 (2013).
- 425 ²Q. Deng, M. Kammoun, A. Erturk, and P. Sharma, "Nanoscale flexoelectric
426 energy harvesting," *Int. J. Solids Struct.* **51**, 3218–3225 (2014).
- 427 ³K. F. Wang and B. L. Wang, "Non-linear flexoelectricity in energy harvesting,"
428 *Int. J. Eng. Sci.* **116**, 88–103 (2017).
- 429 ⁴S. Zhang, K. Liu, M. Xu, and S. Shen, "A curved resonant flexoelectric actuator,"
430 *Appl. Phys. Lett.* **111**, 082904 (2017).
- 431 ⁵U. K. Bhaskar, N. Banerjee, A. Abdollahi, Z. Wang, D. G. Schlom, G. Rijnders,
432 and G. Catalan, "A flexoelectric microelectromechanical system on silicon," *Nat.*
433 *Nanotechnol.* **11**, 263–266 (2016).

- 434 ⁶G. Dong, S. Li, M. Yao, Z. Zhou, Y.-Q. Zhang, X. Han, Z. Luo, J. Yao, B. Peng,
435 Z. Hu, *et al.*, “Super-elastic ferroelectric single-crystal membrane with continuous
436 electric dipole rotation,” *Science* **366**, 475–479 (2019).
- 437 ⁷W. Huang, X. Yan, S. R. Kwon, S. Zhang, F.-G. Yuan, and X. Jiang, “Flexo-
438 electric strain gradient detection using $\text{Ba}_{0.64}\text{Sr}_{0.36}\text{TiO}_3$ for sensing,” *Appl. Phys.*
439 *Lett.* **101**, 252903 (2012).
- 440 ⁸S. Zhang, M. Xu, K. Liu, and S. Shen, “A flexoelectricity effect-based sensor for
441 direct torque measurement,” *J. Phys. D: Appl. Phys.* **48**, 485502 (2015).
- 442 ⁹V. S. Mashkevich and K. B. Tolpygo, “Electrical, optical and elastic properties
443 of diamond type crystals,” *Sov. Phys. JETP* **5**, 435–439 (1957).
- 444 ¹⁰S. M. Kogan, “Piezoelectric effect during inhomogeneous deformation and acous-
445 tic scattering of carriers in crystals,” *Sov. Phys.-Solid State* **5**, 2069–2070 (1964).
- 446 ¹¹V. L. Indenbom, E. B. Loginov, and M. A. Osipov, “Flexoelectric effect and
447 crystal-structure,” *Kristallografiya* **26**, 1157–1162 (1981).
- 448 ¹²V. L. Indenbom, E. B. Loginov, and M. A. Osipov, “The flexoelectric effect and
449 the structure of crystals,” *Sov Phys - Crystallogr.* **26**, 656–8 (1981).
- 450 ¹³A. K. Tagantsev, “Theory of flexoelectric effect in crystals,” *Zh. Eksp. Teor. Fiz.*
451 **88**, 2108–22 (1985).
- 452 ¹⁴A. K. Tagantsev, “Piezoelectricity and flexoelectricity in crystalline dielectrics,”
453 *Phys. Rev. B* **34**, 5883 (1986).
- 454 ¹⁵E. Sahin and S. Dost, “A strain-gradients theory of elastic dielectrics with spatial
455 dispersion,” *Int. J. Eng. Sci.* **26**, 1231–1245 (1988).
- 456 ¹⁶P. Harris, “Mechanism for the shock polarization of dielectrics,” *J. Appl. Phys.*
457 **36**, 739–741 (1965).
- 458 ¹⁷A. Askar, P. C. Y. Lee, and A. S. Cakmak, “Lattice-dynamics approach to the
459 theory of elastic dielectrics with polarization gradient,” *Phys. Rev. B* **1**, 3525–
460 3537 (1970).

- 461 ¹⁸R. Maranganti and P. Sharma, “Atomistic determination of flexoelectric proper-
462 ties of crystalline dielectrics,” *Phys. Rev. B* **80**, 054109 (2009).
- 463 ¹⁹R. Resta, “Towards a bulk theory of flexoelectricity,” *Phys. Rev. Lett.* **105**,
464 127601 (2010).
- 465 ²⁰T. Dumitrică, C. M. Landis, and B. I. Yakobson, “Curvature induced polarization
466 in carbon nanoshells,” *Chem. Phys. Lett.* **360**, 182–188 (2002).
- 467 ²¹S. V. Kalinin and V. Meunier, “Electronic flexoelectricity in low-dimensional
468 systems,” *Phys. Rev. B* **77**, 033403 (2008).
- 469 ²²I. Naumov, A. M. Bratkovsky, and V. Ranjan, “Unusual flexoelectric effect in two-
470 dimensional noncentrosymmetric sp^2 -bonded crystals,” *Phys. Rev. Lett.* **102**,
471 217601 (2009).
- 472 ²³P. J. Mitchell and D. Fincham, “Shell model simulations by adiabatic dynamics,”
473 *J. Phys. Condens. Matter* **5**, 1031 (1993).
- 474 ²⁴M. S. Majdoub, P. Sharma, and T. Cagin, “Enhanced size-dependent piezoelec-
475 tricity and elasticity in nanostructures due to the flexoelectric effect,” *Phys. Rev.*
476 *B* **77**, 125424 (2008).
- 477 ²⁵R. Mbarki, J. B. Haskins, A. Kinaci, and T. Cagin, “Temperature dependence
478 of flexoelectricity in BaTiO_3 and SrTiO_3 perovskite nanostructures,” *Phys. Lett. A*
479 **378**, 2181–2183 (2014).
- 480 ²⁶A. Chatzopoulos, P. Beck, J. Roth, and H.-R. Trebin, “Atomistic modeling of
481 flexoelectricity in periclase,” *Phys. Rev. B* **93**, 024105 (2016).
- 482 ²⁷S. Mao, P. K. Purohit, and N. Aravas, “Mixed finite-element formulations in
483 piezoelectricity and flexoelectricity,” *Proc. R. Soc. A: Math. Phys. Eng. Sci.* **472**,
484 20150879 (2016).
- 485 ²⁸Y. Mao, S. Ai, X. Xiang, and C. Chen, “Theory for dielectrics considering the
486 direct and converse flexoelectric effects and its finite element implementation,”
487 *Appl. Math. Model.* **40**, 7115–7137 (2016).

- 488 ²⁹H. T. Chen, A. K. Soh, and Y. Ni, “Phase field modeling of flexoelectric effects
489 in ferroelectric epitaxial thin films,” *Acta Mech.* **225**, 1323–1333 (2014).
- 490 ³⁰Q. Li, C. T. Nelson, S.-L. Hsu, A. R. Damodaran, L.-L. Li, A. K. Yadav, M. Mc-
491 Carter, L. W. Martin, R. Ramesh, and S. V. Kalinin, “Quantification of flexo-
492 electricity in PbTiO₃/SrTiO₃ superlattice polar vortices using machine learning
493 and phase-field modeling,” *Nat. Commun.* **8**, 1–8 (2017).
- 494 ³¹K. M. Hamdia, H. Ghasemi, X. Zhuang, N. Alajlan, and T. Rabczuk, “Computa-
495 tional machine learning representation for the flexoelectricity effect in truncated
496 pyramid structures,” *Comput. Mater. Contin.* **59**, 79–87 (2019).
- 497 ³²L. Xiang, X. Zeng, X. Huang, and G. Li, “The application of artificial neural-
498 network potentials for flexoelectricity: Performance for anatase-type TiO₂,”
499 *Phys. Lett. A* **384**, 126217 (2020).
- 500 ³³H. Ghasemi, H. S. Park, and T. Rabczuk, “A multi-material level set-based
501 topology optimization of flexoelectric composites,” *Computer Methods in Ap-
502 plied Mechanics and Engineering* **332**, 47–62 (2018).
- 503 ³⁴H. V. Do, T. Lahmer, X. Zhuang, N. Alajlan, H. Nguyen-Xuan, and T. Rabczuk,
504 “An isogeometric analysis to identify the full flexoelectric complex material prop-
505 erties based on electrical impedance curve,” *Computers & Structures* **214**, 1–14
506 (2019).
- 507 ³⁵W. Ma and L. E. Cross, “Large flexoelectric polarization in ceramic lead magne-
508 sium niobate,” *Appl. Phys. Lett.* **79**, 4420–4422 (2001).
- 509 ³⁶W. Ma and L. E. Cross, “Observation of the flexoelectric effect in relaxor
510 Pb(Mg_{1/3}Nb_{2/3})O₃ ceramics,” *Appl. Phys. Lett.* **78**, 2920–2921 (2001).
- 511 ³⁷W. Ma and L. E. Cross, “Flexoelectric polarization of barium strontium titanate
512 in the paraelectric state,” *Appl. Phys. Lett.* **81**, 3440–3442 (2002).
- 513 ³⁸W. Ma and L. E. Cross, “Strain-gradient-induced electric polarization in lead
514 zirconate titanate ceramics,” *Appl. Phys. Lett.* **82**, 3293–3295 (2003).

515 ³⁹W. Ma and L. E. Cross, “Flexoelectric effect in ceramic lead zirconate titanate,”
516 Appl. Phys. Lett. **86**, 072905 (2005).

517 ⁴⁰W. Ma and L. E. Cross, “Flexoelectricity of barium titanate,” Appl. Phys. Lett.
518 **88**, 232902 (2006).

519 ⁴¹J. Narvaez and G. Catalan, “Origin of the enhanced flexoelectricity of relaxor
520 ferroelectrics,” Appl. Phys. Lett. **104**, 162903 (2014).

521 ⁴²L. Shu, W. Huang, S. Ryung Kwon, Z. Wang, F. Li, X. Wei, S. Zhang, M. Lan-
522 gan, X. Yao, and X. Jiang, “Converse flexoelectric coefficient f_{1212} in bulk
523 $\text{Ba}_{0.67}\text{Sr}_{0.33}\text{TiO}_3$,” Appl. Phys. Lett. **104**, 232902 (2014).

524 ⁴³W. Huang, K. Kim, S. Zhang, F.-G. Yuan, and X. Jiang, “Scaling effect of
525 flexoelectric $(\text{Ba}, \text{Sr})\text{TiO}_3$ microcantilevers,” Phys. Status Solidi Rapid Res. Lett.
526 **5**, 350–352 (2011).

527 ⁴⁴A. Kvashnin, P. Sorokin, and B. Yakobson, “Flexoelectricity in carbon nanostruc-
528 tures: Nanotubes, fullerenes, and nanocones,” J. Phys. Chem. Lett. **6**, 2740–4
529 (2015).

530 ⁴⁵S. Chandratre and P. Sharma, “Coaxing graphene to be piezoelectric,” Appl.
531 Phys. Lett. **100**, 023114 (2012).

532 ⁴⁶S. I. Kundalwal, S. A. Meguid, and G. J. Weng, “Strain gradient polarization in
533 graphene,” Carbon **117**, 462–472 (2017).

534 ⁴⁷T. Pandey, L. Covaci, M. V. Milošević, and F. M. Peeters, “Flexoelectricity and
535 transport properties of phosphorene nanoribbons under mechanical bending,”
536 Phys. Rev. B **103**, 235406 (2021).

537 ⁴⁸S. I. Kundalwal, V. K. Choyal, and V. Choyal, “Flexoelectric effect in boron
538 nitride–graphene heterostructures,” Acta Mech. **232**, 3781–3800 (2021).

539 ⁴⁹W. Shi, Y. Guo, Z. Zhang, and W. Guo, “Flexoelectricity in monolayer transition
540 metal dichalcogenides,” J. Phys. Chem. Lett. **9**, 6841–6846 (2018).

541 ⁵⁰W. Shi, Y. Guo, Z. Zhang, and W. Guo, “Strain gradient mediated magnetism
542 and polarization in monolayer vse_2 ,” J. Phys. Chem. C **123**, 24988–24993 (2019).

543 ⁵¹S. Kumar, D. Codony, I. Arias, and P. Suryanarayana, “Flexoelectricity in atomic
544 monolayers from first principles,” *Nanoscale* **13**, 1600–1607 (2021).

545 ⁵²X. Zhuang, B. He, B. Javvaji, and H. S. Park, “Intrinsic bending flexoelectric
546 constants in two-dimensional materials,” *Phys. Rev. B* **99**, 054105 (2019).

547 ⁵³B. Javvaji, B. He, X. Zhuang, and H. S. Park, “High flexoelectric constants in
548 Janus transition-metal dichalcogenides,” *Phys. Rev. Mater.* **3**, 125402 (2019).

549 ⁵⁴Z. Wang and M. Devel, “Electrostatic deflections of cantilevered metallic carbon
550 nanotubes via charge-dipole model,” *Phys. Rev. B* **76**, 195434 (2007).

551 ⁵⁵Z. Wang, M. Zdrojek, T. Mélin, and M. Devel, “Electric charge enhancements in
552 carbon nanotubes: Theory and experiments,” *Phys. Rev. B* **78**, 085425 (2008).

553 ⁵⁶Y. Yang, M. Devel, and Z. Wang, “An atomistic model for the charge distribution
554 in layered MoS₂,” *J. Chem. Phys.* **149**, 124102 (7) (2018).

555 ⁵⁷C. J. Brennan, R. Ghosh, K. Koul, S. K. Banerjee, N. Lu, and E. T. Yu, “Out-of-
556 plane electromechanical response of monolayer molybdenum disulfide measured
557 by piezoresponse force microscopy,” *Nano Lett.* **17**, 5464–5471 (2017).

558 ⁵⁸C. J. Brennan, K. Koul, N. Lu, and E. T. Yu, “Out-of-plane electromechanical
559 coupling in transition metal dichalcogenides,” *Appl. Phys. Lett.* **116**, 053101
560 (2020).

561 ⁵⁹M. L. Olson and K. R. Sundberg, “An atom monopole–dipole interaction model
562 with charge transfer for the treatment of polarizabilities of π -bonded molecules.”
563 *J. Chem. Phys.* **69**, 5400–5404 (1978).

564 ⁶⁰A. Mayer, P. Lambin, and R. Langlet, “Charge-dipole model to compute the
565 polarization of fullerenes,” *Appl. Phys. Lett.* **89**, 063117 (2006).

566 ⁶¹A. Mayer, “Formulation in terms of normalized propagators of a charge-dipole
567 model enabling the calculation of the polarization properties of fullerenes and
568 carbon nanotubes,” *Phys. Rev. B* **75**, 045407 (2007).

569 ⁶²A. Mayer and P.-O. Åstrand, “A charge-dipole model for the static polarizability
570 of nanostructures including aliphatic, olephinic, and aromatic systems,” *J. Phys.*

571 Chem. A **112**, 1277–1285 (2008).

572 ⁶³A. Mayer, A. L. Gonzalez, C. M. Aikens, and G. C. Schatz, “A charge–dipole
573 interaction model for the frequency-dependent polarizability of silver clusters,”
574 Nanotechnology **20**, 195204 (2009).

575 ⁶⁴L. Jensen, P. O. Åstrand, A. Osted, J. Kongsted, and K. V. Mikkelsen, “Polar-
576 izability of molecular clusters as calculated by a dipole interaction model,” J.
577 Chem. Phys. **116**, 4001–4010 (2002).

578 ⁶⁵R. Langlet, M. Devel, and P. Lambin, “Computation of the static polarizabilities
579 of multi-wall carbon nanotubes and fullerenes using a Gaussian regularized point
580 dipole interaction model,” Carbon **44**, 2883–2895 (2006).

581 ⁶⁶X. Li and H. Zhu, “Two-dimensional MoS₂: Properties, preparation, and appli-
582 cations,” J. Materiomics **1**, 33–44 (2015).

583 ⁶⁷M. Wen, S. N. Shirodkar, P. Plecháč, E. Kaxiras, R. S. Elliott, and E. B. Tadmor,
584 “A force-matching Stillinger-Weber potential for MoS₂: Parameterization and
585 Fisher information theory based sensitivity analysis,” J. Appl. Phys. **122**, 244301
586 (2017).

587 ⁶⁸M. Madziarz, “Transferability of molecular potentials for 2D molybdenum disul-
588 phide,” Materials **14**, 519 (2021).

589 ⁶⁹H. Hirakata, Y. Fukuda, and T. Shimada, “Flexoelectric properties of multilayer
590 two-dimensional material MoS₂,” J. Phys. D: Appl. Phys. **55**, 125302 (2021).

591 ⁷⁰Y. Lee, S. Park, H. Kim, G. H. Han, Y. H. Lee, and J. Kim, “Characteriza-
592 tion of the structural defects in CVD-grown monolayered MoS₂ using near-field
593 photoluminescence imaging,” Nanoscale **7**, 11909–11914 (2015).

594 ⁷¹M. Springolo, M. Royo, and M. Stengel, “Direct and converse flexoelectricity in
595 two-dimensional materials,” Phys. Rev. Lett. **127**, 216801 (2021).

596 ⁷²B. Wang, Y. Gu, S. Zhang, and L.-Q. Chen, “Flexoelectricity in solids: Progress,
597 challenges, and perspectives,” Prog. Mater. Sci **106**, 100570 (2019).

598 ⁷³J. Hong, G. Catalan, J. F. Scott, and E. Artacho, “The flexoelectricity of barium
599 and strontium titanates from first principles,” *J. Phys. Condens. Matter* **22**,
600 112201 (2010).

601 ⁷⁴W. Hao, Z. Wu, X. Li, and Y. Pu, “Edge effect on flexoelectronic properties of
602 Janus MoSSe nanoribbons: A first-principles study,” *J. Appl. Phys.* **129**, 185101
603 (2021).